An Arbitrary-Order Discontinuous Galerkin Method with One Unknown Per Element

Ruo Li, Pingbing Ming, Ziyuan Sun & Zhijian Yang

Journal of Scientific Computing

ISSN 0885-7474
Volume 80
Number 1

J Sci Comput (2019) 80:268-288
DOI 10.1007/s10915-019-00937-y

Springer

Journal of Scientific Computing (2019) 80:268–288
https://doi.org/10.1007/s10915-019-00937-y

An Arbitrary-Order Discontinuous Galerkin Method with One Unknown Per Element

Ruo Li[1] · Pingbing Ming[2,3] · Ziyuan Sun[4] · Zhijian Yang[5]

Received: 19 October 2018 / Revised: 27 February 2019 / Accepted: 5 March 2019 /
Published online: 14 March 2019

Abstract
We propose an arbitrary-order discontinuous Galerkin method for second-order elliptic problem on general polygonal mesh with only one degree of freedom per element. This is achieved by locally solving a discrete least-squares over a neighboring element patch. Under a geometrical condition on the element patch, we prove an optimal a priori error estimates in the energy norm and in the L^2 norm. The accuracy and the efficiency of the method up to order six on several polygonal meshes are illustrated by a set of benchmark problems.

Keywords Least-squares reconstruction · Discontinuous Galerkin method · Elliptic problem

Mathematics Subject Classification Primary 65N30 · 49N45; Secondary 74K20

1 Introduction

The discontinuous Galerkin method (DG) [18,43] is by now a very standard numerical method to simulate a wide variety of partial differential equations of scientific and engineering inter-

✉ Pingbing Ming
mpb@lsec.cc.ac.cn

Ruo Li
rli@math.pku.edu.cn

Ziyuan Sun
zysun@math.pku.edu.cn

Zhijian Yang
zjyang.math@whu.edu.cn

1 CAPT, LMAM and School of Mathematical Sciences, Peking University, Beijing 100871, People's Republic of China

2 LSEC, Academy of Mathematics and Systems Science, Chinese Academy of Sciences, No. 55, Zhong-Guan-Cun East Road, Beijing 100190, People's Republic of China

3 School of Mathematical Sciences, University of Chinese Academy of Sciences, No. 19A, Yu-Quan Road, Beijing 100049, People's Republic of China

4 School of Mathematical Sciences, Peking University, Beijing 100871, People's Republic of China

5 School of Mathematics and Statistics, Wuhan University, Wuhan 430072, People's Republic of China

est. Recently there are quite a few works concerning the discontinuous Galerkin method on general polytopic (polygonal or polyhedral) meshes [2,12–14,22,30,36,50]. Unlike the finite element method [45], the full discontinuity across the element interfaces of the trial and test function spaces of DG method lends itself naturally to the polytopic meshes, which does provide more flexibility in implementation, in particular for domain with microstructures or problems with certain physical constraints. Such meshes may ease the triangulation of complex domains or domains with microstructures. On the other hand, compared to the classical finite element method, the DG method is computationally expensive over a particular computational mesh and approximation order, which is due to the rapid increasing of the local degrees of freedom. Moreover, for certain problems such as fluid solid interaction problems or a heat diffusion problem that is coupled or is embedded into a compressible fluid problem, there is no enough information to support a large number of local degrees of freedom. Though this problem is partially solved by the agglomeration-based physical frame DG method [7,8] and the hybrid DG method [19], it is desirable to develop a DG method with less local degrees of freedom while retaining high accuracy.

A common trait is to employ patch reconstruction to achieve high accuracy. To the best of the authors' knowledge, such reconstruction idea can be traced back to the endeavors on developing three node plate bending elements and simple shell elements in the early 1970s; see, e.g., [29,40–42]. Similar ideas may also be found in WENO [47] and finite volume method for hyperbolic conservation laws [6].

This motivates us to use patches of a piecewise constant function to reconstruct a piecewise high order polynomial on each element, which is achieved by solving a discrete least-squares problem over element patch. Such approach has been used in [32] to reconstruct piecewise effective tensor field from scattered data for the multiscale partial differential equations. This new space is a sub-space of the commonly used approximation space of DG method, which may be combined with various DG variational formulations to numerically solve even more general elliptic problems such as plate bending problem [33], Stokes flow problems [35], and eigenvalue problems [34], just name a few. As a starting point, we employ the Interior Penalty discontinuous Galerkin (IPDG) method [3] with this reconstructed approximation space to solve Poisson problem. Under a mild condition on the geometry of the element patch, we proved that this reconstructed approximation space admits optimal approximation order in certain broken Sobolev norms, by which we derived the optimal error estimates in the DG-energy norm and in the L^2 norm for the proposed method.

Our method possesses several attractive features. First, arbitrary order accuracy may be achieved with increasing the order of the reconstruction, while there is only one degree of freedom per element, by contrast to the standard DG method, which requires at least three unknowns on each element. From this aspect of view, the proposed method has a flavor of finite volume method. Second, the method can be used on any shape of elements, which may be triangles, quadrilaterals, polygons in two dimension, or tetrahedron, prism, pyramid, hexahedron in three dimension. In particular, the method may be used on the hybrid mesh, which is nowadays quite common in simulations because it can handle the complicated domain or even reduce the total number of unknowns [51]. Third, the reconstruction procedure of the proposed method is stable with respect to the small perturbation of the data, which is of practical interesting due to the measurement error. Moreover, our results for the reconstruction operator is of independent interest for the discrete least-squares [44] and some other recovery type method [28].

A closely related approach is a DG method proposed in [31]. The authors introduced a family of continuous linear finite elements for the Kirhhoff–Love plate model. A continuous linear interpolation of the deflection field is employed to reconstruct a discontinuous

quadratic deflection field by solving a local least-squares problem over element patch. It is worth mentioning that one of their reconstruction method is the same with the second order constrained reconstruction in [32]. Moreover, this method only applies to structured mesh. Another related method is the cell-centered Galerkin method presented in [23]. The authors developed an arbitrary-order discretization method of diffusion problems on general polyhedral mesh. The cornerstone of this method is the locally reconstructed discrete gradient operator and a stabilized term, while our method is the locally reconstructed finite element space. The so-called R-FEM [25] is similar to the proposed method in the sense that it also constructed via a recovery operator over a piecewise discontinuous approximation space. The reconstruction is based on certain Clément type averaging operator [17]. The difference between R-FEM and the present method lies in the fact that the reconstructed space of R-FEM is conforming or non-conforming, while ours is totally discontinuous across the element boundaries. Moreover, R-FEM needs an extra stabilized term for the well-posedness of the variational problem as that in [23]. R-FEM essentially bears certain similarities with a linear conforming finite element for biharmonic problem and corresponding eigenvalue problem [15,28], which is based on the remarkable polynomial preserving reconstruction operator, while R-FEM has not been applied to higher-order elliptic problems so far. Another closely related method is the Galerkin difference method proposed by Banks and Hagstrom [5], high order difference schemes are constructed in a Galerkin framework. The underlying basis functions are Lagrange functions associated with continuous piecewise polynomial approximation on a computational grid, while the basis function in the proposed method is discontinuous.

The rest of the paper is organized as follows. In Sect. 2, we describe the reconstruction finite element space and prove its approximation properties and the stability properties of the reconstruction. In Sect. 3, we present the interior penalty discontinued Galerkin method for Poisson problem with the reconstructed approximation space and prove a priori error estimate, and in Sect. 4, numerical results for second order elliptic problems in two dimension are presented. Finally, in Sect. 5, we summarize the work and draw some conclusions.

Throughout this paper, we shall use standard notations for Sobolev spaces, norms and seminorms [1]; see, e.g.,

$$\|u\|_{H^1(D)} := \left(\| u \|^2_{L^2(D)} + \| \nabla u \|^2_{L^2(D)} \right)^{1/2}$$

for any bounded domain D. We use C as a generic constant independent of the mesh size, which may change from line to line. We shall focus on two dimensional problem though most results are valid in three dimension.

2 Approximation Space

Let Ω be a polygonal domain in $\mathbb{R}^2$. The mesh $\mathcal{T}_h$ is a triangulation of Ω with polygons K, which may not be convex. Here $h := \max_{K \in \mathcal{T}_h} h_K$ with h_K the diameter of K. We denote $|K|$ the area of K. Let $\mathbb{P}_m(D)$ be a set of polynomial in two variables with total degree at most m confined to domain D, where D may be an element K or an agglomeration of the elements belong to $\mathcal{T}_h$. We assume that the mesh $\mathcal{T}_h$ satisfies the following shape regularity conditions, which were introduced originally in [11] to study the convergence of mimetic finite difference. Detailed discussion on such conditions may be found in [20, §1.6].

There exist

1. an integer number N independent of h;

2. a real positive number σ independent of h;
3. a compatible sub-decomposition $\widetilde{\mathcal{T}}_h$

such that

A1 any element K admits a decomposition $\widetilde{\mathcal{T}}_h|_K$ that consists of at most N triangles τ.
A2 Any $\tau \in \widetilde{\mathcal{T}}_h$ is shape-regular in the sense of Ciarlet-Raviart [16]: there exists σ such that $h_\tau/\rho_\tau \le \sigma$, where h_τ is the diameter of τ and ρ_τ is the radius of the largest ball inscribed in τ.

Assumptions **A1** and **A2** impose quite weak constraints on the triangulation, which may contain elements with quite general shapes, for example, non-convex or degenerate elements are allowed.

The above shape regularity assumptions lead to some useful consequences, which will be extensively used in the later analysis.

M1 For any $\tau \in \widetilde{\mathcal{T}}_h$, there exists $\rho_1 \ge 1$ that depends on N and σ such that $h_K/h_\tau \le \rho_1$.
M2 [*Agmon inequality*] For all $v \in H^1(K)$, there exists C that depends on N and σ, but independent of h_K such that,

$$\| v \|^2_{L^2(\partial K)} \le C \left(h_K^{-1} \| v \|^2_{L^2(K)} + h_K \| \nabla v \|^2_{L^2(K)} \right). \tag{2.1}$$

M3 [*Approximation property*] For any positive integer m, there exists C that depends on N, m and σ, but independent of h_K such that for any $v \in H^{m+1}(K)$, there exists an approximation polynomial $\widetilde{v} \in \mathbb{P}_m(K)$ such that

$$\| v - \widetilde{v} \|_{L^2(K)} + h_K \| \nabla(v - \widetilde{v}) \|_{L^2(K)} \le C h_K^{m+1} | v |_{H^{m+1}(K)}. \tag{2.2}$$

M4 [*Inverse inequality*] For any $v \in \mathbb{P}_m(K)$, there exists a constant C that depends only on N, m, σ and ρ_1 such that

$$\| \nabla v \|_{L^2(K)} \le C h_K^{-1} \| v \|_{L^2(K)}. \tag{2.3}$$

We have not list all the mesh conditions in [11] and [20, §1.6], while the above two Assumptions **A1** and **A2** suffice for our purpose. **M1** may be proved as follows. Since the sub-triangulation $\widetilde{\mathcal{T}}_h$ is shape-regular and the number of triangles in $\mathcal{T}_h|_K$ is bounded by N, there holds

$$\min_{\tau \in \widetilde{\mathcal{T}}_h|_K} h_\tau \ge \sigma^{-N} \max_{\tau \in \widetilde{\mathcal{T}}_h} h_\tau. \tag{2.4}$$

Without loss of generality, we assume that $h_{\tau'} = \min_{\tau \in \widetilde{\mathcal{T}}_h|_K} h_\tau$ and $h_{\tau''} = \max_{\tau \in \widetilde{\mathcal{T}}_h} h_\tau$. Note that the sub-triangulation $\widetilde{\mathcal{T}}_h$ is shape-regular, there exists $n \in \mathbb{N}$ such that for $i = 1, \ldots, n$,

$$\tau_0 = \tau', \quad \tau_n = \tau'', \quad \overline{\tau}_i \cap \overline{\tau}_{i-1} = e_i$$

with e_i the common edge of τ_i and τ_{i-1}. This implies that for any $i = 1, \ldots, n$, there holds

$$h_{\tau_i} \le \sigma \rho_{\tau_i} \le \sigma |e_i| \le \sigma h_{\tau_{i-1}}.$$

Therefore, we obtain

$$\frac{h_{\tau''}}{h_{\tau'}} = \prod_{i=1}^{n} \frac{h_{\tau_i}}{h_{\tau_{i-1}}} \le \sigma^n \le \sigma^N.$$

This gives (2.4).

Note that

$$h_K \le \sum_{\tau\in\widetilde{\mathcal{T}}_h|_K} h_\tau \le N \max_{\tau\in\widetilde{\mathcal{T}}_h} h_\tau = N h_{\tau''}.$$

Therefore, **M1** follows with $\rho_1 = N\sigma^N$.

The *Agmon inequality* **M2** and the *Approximation property* **M3** have been proved in [20, §1.6.3].

The *inverse inequality* **M4** may be proved as follows. For any $v \in \mathbb{P}_m(K)$, the restriction $v|_\tau \in \mathbb{P}_m(\tau)$, using the following standard inverse inequality on triangle τ [16], we have

$$\| \nabla v \|_{L^2(\tau)} \le C_{\text{inv}} h_\tau^{-1} \| v \|_{L^2(\tau)}.$$

where C_{inv} depends on σ and m while is independent of h_τ. Summing up all $\tau \in \widetilde{T}_h|_K$, and using **M1**, we obtain

$$\begin{aligned}\| \nabla v \|^2_{L^2(K)} &= \sum_{\tau\subset\widetilde{\mathcal{T}}_h|_K} \| \nabla v \|^2_{L^2(\tau)} \le C^2_{\text{inv}}\rho_1^2 h_K^{-2} \sum_{\tau\subset\widetilde{\mathcal{T}}_h|_K} \| v \|^2_{L^2(\tau)} \\ &= C^2_{\text{inv}}\rho_1^2 h_K^{-2} \| v \|^2_{L^2(K)}.\end{aligned}$$

This gives (2.3) with $C = C_{\text{inv}}\rho_1$.

A combination of (2.1) and (2.3) yields the *inverse trace inequality*: For any $v \in \mathbb{P}_r(K)$,

$$\| v \|_{L^2(\partial K)} \le C\,(1 + C_{\text{inv}}\rho_1)\, h_K^{-1/2} \| v \|_{L^2(K)}. \tag{2.5}$$

Remark 1 The above four inequalities (2.1), (2.2), (2.3) and (2.5) are the foundation to derive the error estimate for the IPDG method [3,4], which are also valid over the polygonal meshes satisfying some other shape-regular conditions; see, e.g., [22, §1.4] and [38].

2.1 Reconstruction Operator

Given the triangulation $\mathcal{T}_h$, we define the reconstruction operator in a piecewise manner as follows. For each element $K \in \mathcal{T}_h$, we firstly assign a sampling node $x_K \in K$ that is preferably in the interior of K, and construct an element patch $S(K)$. There are many different ways to find the sampling nodes and construct the element patch. For example, we may let the barycenter of the element K to be the sampling node, while it can be more flexible due to the stability property of the least-squares reconstruction; cf. Lemma 2.

The element patch $S(K)$ usually contains K and some elements around K, which may be built up in the following two ways. The first way is that we initialize $S(K)$ as K, and add all the Moore neighbors [46] (elements with nonempty intersection with the closure of K) into $S(K)$ recursively until sufficiently large number of elements are collected into $S(K)$. This procedure may be recursively defined as follows. For any $t \in \mathbb{N}$, we define

$$S_0(K) := K, \quad S_t(K) := \{\, K \in \mathcal{T}_h \mid \overline{K} \cap \overline{S_{t-1}(K)} \ne \emptyset\}. \tag{2.6}$$

A plot of the element patch by this way may be found in Fig. 1. Such kind of construction has been used in [32] to reconstruct effective tensor field from scattered data.

An alternative way is to use the Von Neumann neighbor [46] (adjacent edge-neighboring elements) instead of the Moore neighbor. Firstly, a threshold value c_0 is assigned to control the size of the patch, which is determined by the cardinality of the local degrees of freedom of the reconstructed polynomial. Secondly, we initialize $S(K)$ as element K itself. Thirdly, all the Von Neumann neighbors of current geometry $S(K)$ are the candidates, we calculate

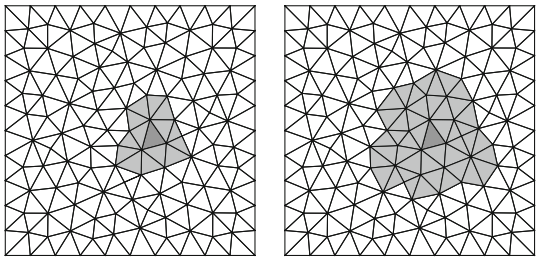

Fig. 1 Patch with Moore neighbors. Left: $S_1(K)$; Right: $S_2(K)$)

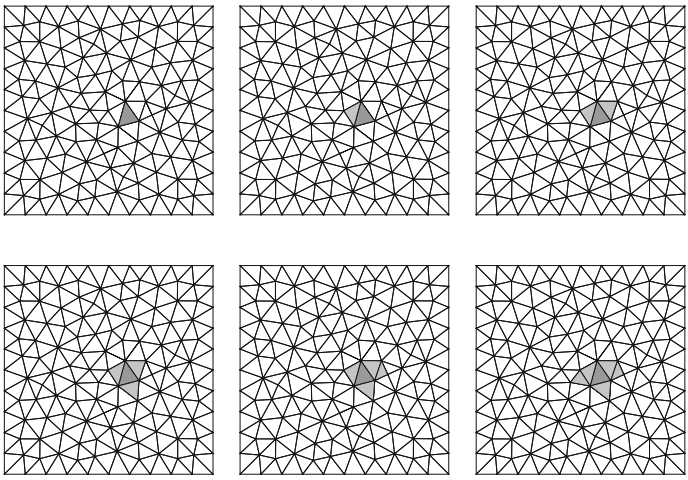

Fig. 2 Patch with Von Neumann neighbors, the threshold $c_0 = 6$

the distances between the sampling nodes of all these candidates and the sampling node inside K, and we include the element with the nearest distance into the patch $S(K)$. Last, the recursive process is terminated until the number of the elements attains the threshold c_0. Such construction is shown in the Fig. 2. Note that we do not make any assumption on the threshold c_0 right now, which will be prescribed in practice; see Sect. 4.

We denote by $\mathcal{I}(K)$ the set of the sampling nodes belonging to $S(K)$ with $\#\mathcal{I}(K)$ its cardinality, and let $\#S(K)$ be the number of elements belonging to $S(K)$. In what follows we choose the barycenter of each element as the sampling point. Hence, $\#\mathcal{I}(K) = \#S(K)$. An example for $S(K)$ and $\mathcal{I}(K)$ is shown in Fig. 3. An upper bound for $\#\mathcal{I}(K)$ may be found in Lemma 6. In view of the construction, the element patch with the Von Neumann neighbors has much smaller $\#S(K)$ than that with the Moore neighboring. Therefore, we use the second approach in all our numerical examples in Sect. 4. Moreover, we define $d_K := \operatorname{diam} S(K)$ and $d = \max_{K \in \mathcal{T}_h} d_K$.

We assume that $S(K)$ satisfies the following geometrical assumption.

Assumption A For every $K \in \mathcal{T}_h$, there exist constants R and r that are independent of K such that $B_r \subset S(K) \subset B_R$ with $R \geq 2r$, and $S(K)$ is star-shaped with respect to B_r, where B_ρ is a disk with radius ρ.

As a direct consequence of the above assumption, we have the following characterization of $S(K)$.

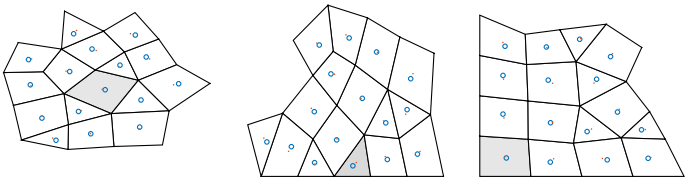

Fig. 3 The element patches $S(K)$ in the interior of the domain (left), along the boundary of the domain (middle) and at the corner of the domain (right), together with randomly perturbed sampling points for Example 3 in Sect. 4. Here the element K is marked in black and the sampling nodes in $\mathcal{I}(K)$ are the barycenters of the elements, which are marked in dots, and the perturbed sampling nodes in $\widetilde{\mathcal{I}}(K)$ are marked as small circles

Lemma 1 *If* **Assumption A** *is valid, then $S(K)$ satisfies an interior cone condition, and there exists a uniform bound γ for the chunkiness parameter of $S(K)$.*

Proof By [39, Proposition 2.1], if **Assumption A** holds true, then the element patch $S(K)$ satisfies an interior cone condition with radius r and angel $\theta = 2\arcsin\dfrac{r}{2R}$.

By definition [9, Definition 4.2.16], the chunkiness parameter γ_K is defined as the ratio between the diameter of $S(K)$ and the radius of the largest ball to which $S(K)$ is star-shaped. This leads to the following bound

$$\gamma_K := \frac{d_K}{r} \le \frac{2R}{r}.$$

Let $\gamma := 2R/r$, we obtain a uniform bound on the chunkiness parameter for all $K \in \mathcal{T}_h$. □

Let U_h be the piecewise constant space associated with $\mathcal{T}_h$, i.e.,

$$U_h := \{\, v \in L^2(\Omega) \;\mid\; v|_K \in \mathbb{P}_0(K)\}.$$

For any $v \in U_h$ and for any $K \in \mathcal{T}_h$, we reconstruct a high order polynomial $\mathcal{R}_K v$ of degree m by solving the following discrete least-squares.

$$\mathcal{R}_K v = \operatorname{argmin}_{p\in\mathbb{P}_m(S(K))} \sum_{x\in\mathcal{I}(K)} |v(x) - p(x)|^2 . \tag{2.7}$$

A global reconstruction operator $\mathcal{R}$ is defined by $\mathcal{R}|_K = \mathcal{R}_K$. Given $\mathcal{R}$, we embed U_h into a discontinuous finite element space with piecewise polynomials of degree m, and denote $V_h = \mathcal{R}U_h$.

In what follows, we make the following assumption on the sampling node set $\mathcal{I}(K)$.

Assumption B For any $K \in \mathcal{T}_h$ and $p \in \mathbb{P}_m(S(K))$,

$$p|_{\mathcal{I}(K)} = 0 \quad \text{implies} \quad p|_{S(K)} \equiv 0. \tag{2.8}$$

This assumption implies the uniqueness, and equally the existence of the discrete least-squares (2.7). **Assumption B** requires that $\#\mathcal{I}(K)$ cannot be too small, which is at least $(m+2)(m+1)/2$ to guarantee the unisolvence of the discrete least-squares. A quantitative version of this assumption is

$$\Lambda(m, \mathcal{I}(K)) < \infty$$

with

$$\Lambda(m, \mathcal{I}(K)) := \max_{p\in\mathbb{P}_m(S(K))} \frac{\| p \|_{L^\infty(S(K))}}{\| p|_{\mathcal{I}(K)} \|_{\ell_\infty}}. \tag{2.9}$$

The reconstruction procedure is robust with respect to the small perturbation of the sampling nodes due to the following stability result. In particular, $\Lambda(m, \mathcal{I}(K))$ remains bounded with respect to small perturbation. This problem is of practical interest because both the sampled values and the positions of the sampling nodes are affected by the measurable errors.

Lemma 2 *Let $S(K)$ be the element patch defined above and $g \in C^1(S(K))$. If we assume that*

1. *There exists $\alpha > 0$ such that*

$$\| g \|_{L^\infty(S(K))} \leq \alpha \| g|_{\mathcal{I}(K)} \|_{\ell_\infty}. \tag{2.10}$$

2. *$S(K)$ admits a Markov-type inequality in the sense that there exists $\beta > 0$ such that*

$$\| \nabla g \|_{L^\infty(S(K))} \leq \beta \| g \|_{L^\infty(S(K))}. \tag{2.11}$$

Then for any $\delta \in (0, 1)$, there exists $\varepsilon = \delta/(\alpha\beta)$ such that for any sampling node set $\widetilde{\mathcal{I}}(K)$ that is a perturbation of $\mathcal{I}(K)$ in the sense that $\widetilde{\mathcal{I}}(K) \subset \mathcal{I}(K) + B(0, \varepsilon)$ with B centers at 0 with radius ε, the following stability estimate is valid:

$$\| g \|_{L^\infty(S(K))} \leq \frac{\alpha}{1-\delta} \| g|_{\widetilde{\mathcal{I}}(K)} \|_{\ell_\infty}. \tag{2.12}$$

This stability estimate for the reconstruction procedure depends on the assumptions (2.10) and (2.11). The validity of these two assumptions hinges on certain geometrical condition on the element patch. For example, if the element patch $S(K)$ is convex, then by [32, Lemma 3.5], the first assumption (2.10) is valid with $\alpha = 2$, and the second assumption (2.11) is valid for $g \in \mathbb{P}_m(S(K))$ with $\beta = 4m^2/w(K)$ due to the *Markov inequality* of Wilhelmsen [49] for the convex domain $S(K)$, where $w(K)$ is the width of $S(K)$. A more general condition for the validity of these two assumptions may be found in Remark 3.

Proof Let $x^* \in \mathcal{I}(K)$ satisfy $|g(x^*)| = \| g|_{\mathcal{I}(K)} \|_{\ell_\infty}$. There exists $\widetilde{x} \in \widetilde{\mathcal{I}}(K)$ such that $|\widetilde{x} - x^*| \leq \varepsilon$. By Taylor's expansion,

$$\begin{aligned} \left|g(x^*)\right| &\leq |g(\widetilde{x})| + \varepsilon \max_{x \in S(K)} |\nabla g(x)| \\ &\leq \| g|_{\widetilde{\mathcal{I}}(K)} \|_{\ell_\infty} + \varepsilon\beta \| g \|_{L^\infty(S(K))}, \end{aligned}$$

where we have used the Markov's inequality (2.11). Combining the above inequality and (2.10), we obtain

$$\begin{aligned} \| g \|_{L^\infty(S(K))} &\leq \alpha \| g|_{\mathcal{I}(K)} \|_{\ell_\infty} = \alpha \left|g(x^*)\right| \\ &\leq \alpha \| g|_{\widetilde{\mathcal{I}}(K)} \|_{\ell_\infty} + \varepsilon\alpha\beta \| g \|_{L^\infty(S(K))} \\ &= \alpha \| g|_{\widetilde{\mathcal{I}}(K)} \|_{\ell_\infty} + \delta \| g \|_{L^\infty(S(K))}, \end{aligned}$$

which immediately implies the stability estimate (2.12). □

The following properties of the reconstruction operator $\mathcal{R}_K$ is proved in [32, Theorem 3.3], which is of vital importance to our error estimate.

Lemma 3 *If* **Assumption B** *holds, then there exists a unique solution of (2.7) for any $K \in \mathcal{T}_h$. The unique solution is denoted by $\mathcal{R}_K v$.*

Moreover $\mathcal{R}_K$ satisfies

$$\mathcal{R}_K g = g \quad \text{for all} \quad g \in \mathbb{P}_m(S(K)). \tag{2.13}$$

The stability property holds true for any $K \in \mathcal{T}_h$ *and* $g \in C^0(S(K))$ *as*

$$\| \mathcal{R}_K g \|_{L^\infty(K)} \leq \Lambda(m, \mathcal{I}(K)) \sqrt{\#\mathcal{I}(K)} \| g|_{\mathcal{I}(K)} \|_{\ell_\infty}, \tag{2.14}$$

and the quasi-optimal approximation property is valid in the sense that

$$\| g - \mathcal{R}_K g \|_{L^\infty(K)} \leq \Lambda_m \inf_{p \in \mathbb{P}_m(S(K))} \| g - p \|_{L^\infty(S(K))}, \tag{2.15}$$

where $\Lambda_m := \max_{K \in \mathcal{T}_h} \{1 + \Lambda(m, \mathcal{I}(K)) \sqrt{\#\mathcal{I}(K)}\}$.

By (2.15), we conclude that the reconstruction $\mathcal{R}_K g$ is a nearly optimal uniform approximation polynomial to g provided that $\Lambda(m, \mathcal{T}(K)) \sqrt{\#\mathcal{I}(K)}$ can be bounded. As a direct consequence of this property, we shall prove below that such nearly optimal approximation property of the reconstruction is also valid with respect to the broken H^1-norm.

Lemma 4 *If* **Assumption B** *holds, then there exists* C *that depends on* N, σ, m *and* γ *such that*

$$\| g - \mathcal{R}_K g \|_{L^2(K)} \leq C \Lambda_m h_K d_K^m | g |_{H^{m+1}(S(K))}. \tag{2.16}$$

$$\| \nabla(g - \mathcal{R}_K g) \|_{L^2(K)} \leq C \left(h_K^m + \Lambda_m d_K^m \right) | g |_{H^{m+1}(S(K))}. \tag{2.17}$$

Proof By Lemma 1, the element patch is star-shaped with respect to a disk B_r with a uniform chunkiness parameter, using [24, Theorem 3.2], we take $p = Q^{m+1} g \in \mathbb{P}_m$ in the right-hand side of (2.15), where $Q^{m+1} g$ is the averaged Taylor polynomial of degree $m+1$. Hence,

$$\begin{aligned} \inf_{p \in \mathbb{P}_m(S(K))} \| g - p \|_{L^\infty(S(K))} &\leq \| g - Q^{m+1} g \|_{L^\infty(S(K))} \\ &\leq C d_K^m | g |_{H^{m+1}(S(K))}, \end{aligned} \tag{2.18}$$

where C depends on N, m, σ and γ.

Substituting the above estimate (2.18) into (2.15), we obtain

$$\| g - \mathcal{R}_K g \|_{L^2(K)} \leq |K|^{1/2} \| g - \mathcal{R}_K g \|_{L^\infty(K)} \leq C \Lambda_m h_K d_K^m | g |_{H^{m+1}(S(K))}.$$

This gives (2.16).

Next, let $\widehat{g}_m$ be the approximation polynomial in (2.2) for function g, using the *inverse inequality* (2.3) and the approximation estimate (2.16), we obtain

$$\begin{aligned} \| \nabla(g - \mathcal{R}_K g) \|_{L^2(K)} &\leq \| \nabla(g - \widehat{g}_m) \|_{L^2(K)} + \| \nabla(\widehat{g}_m - \mathcal{R}_K g) \|_{L^2(K)} \\ &\leq C h_K^m | g |_{H^{m+1}(K)} + C h_K^{-1} \| \widehat{g}_m - \mathcal{R}_K g \|_{L^2(K)} \\ &\leq C h_K^m | g |_{H^{m+1}(K)} + C h_K^{-1} \| g - \widehat{g}_m \|_{L^2(K)} \\ &\quad + C h_K^{-1} \| g - \mathcal{R}_K g \|_{L^2(K)} \\ &\leq C \left(h_K^m + \Lambda_m d_K^m \right) | g |_{H^{m+1}(S(K))}. \end{aligned}$$

This gives (2.17) and completes the proof.

Remark 2 If the element patch $S(K)$ is convex, then the constants C in the right hand side of (2.16) and (2.17) are independent of the chunkiness parameter γ as proven in [21].

The above lemma indicates that the approximation accuracy of the reconstruction procedure boils down to the boundedness of Λ_m. We shall seek for conditions of the triangulation $\mathcal{T}_h$, under which Λ_m is uniformly bounded. The authors in [32] have proved that if the element patch $S(K)$ is convex and the triangulation is quasi-uniform, then Λ_m is uniformly

bounded. However, both conditions are not so realistic in implementation. In next lemma, we shall show that **Assumption A** is more suitable in practice, under which $\Lambda(m, \mathcal{I}(K))$ is also uniformly bounded, which together with the estimate of $\#\mathcal{I}(K)$ in Lemma 6 implies that Λ_m is uniformly bounded.

Lemma 5 *If* **Assumption A** *holds, then for any* $\varepsilon > 0$*, if*

$$r > m\sqrt{2Rh_K(1 + 1/\varepsilon)},$$

then we may take $\Lambda(m, \mathcal{I}(K))$ *as*

$$\Lambda(m, \mathcal{I}(K)) = 1 + \varepsilon. \tag{2.19}$$

Moreover, if $r > 2m\sqrt{Rh_K}$*, we may take* $\Lambda(m, \mathcal{I}(K)) = 2$.

If **Assumption A** is valid, we usually have $R \simeq th_K$. The above result suggests that $r \simeq m\sqrt{th_K}$ for the uniform boundedness of $\Lambda(m, \mathcal{I}(K))$.

By [27, Theorem 1.2.2.2. and Corollary 1.2.2.3], any convex domain satisfies the uniform cone property. Therefore, Lemma 5 generalizes the corresponding result in [32, Lemma 3.5] because it applies to more general element patch.

Proof of Lemma 5 Let $x^* \in \overline{S(K)}$ such that $|p(x^*)| = \max_{x\in\overline{S(K)}} |p(x)|$, and $x_\ell \in \mathcal{I}(K)$ such that $|x_\ell - x^*| = \min_{y\in\mathcal{I}(K)} |x^* - y|$. Then

$$\left|x_\ell - x^*\right| \le h_K/2.$$

By Taylor's expansion, we have

$$p(x_\ell) = p(x^*) + (x_\ell - x^*) \cdot \nabla p(\xi_x)$$

with ξ_x a point on the line with end points x_ℓ and x^*. This gives

$$\left|p(x^*)\right| \le |p(x_\ell)| + \frac{h_K}{2} \max_{x\in S(K)} |\nabla p(x)|\,.$$

By Lemma 1, the element patch $S(K)$ satisfies an interior cone condition with radius r and aperture $\theta = 2\arcsin(r/2R)$. By [48, Proposition 11.6], we have the following Markov inequality:

$$\| \nabla p \|_{L^\infty(S(K))} \le \frac{2m^2}{r \sin\theta} \| p \|_{L^\infty(S(K))} \quad \text{for all} \quad p \in \mathbb{P}_m(S(K)). \tag{2.20}$$

Using the fact that $\theta/2 \le \pi/6$, we have

$$\sin\theta = 2\sin\frac{\theta}{2}\cos\frac{\theta}{2} = 2\frac{r}{2R}\cos\frac{\theta}{2} \ge \frac{r}{2R}.$$

Combining the above three inequalities, we obtain

$$\| p \|_{L^\infty(S(K))} \le \| p|_{\mathcal{I}(K)} \|_{\ell_\infty} + \frac{2m^2 Rh_K}{r^2} \| p \|_{L^\infty(S(K))},$$

which together with the condition on r yields (2.19). □

Remark 3 If **Assumption A** is true, then assumptions (2.10) and (2.11) in Lemma 2 are valid with $\alpha = 1 + \varepsilon$ and $\beta = 2m^2/(r \sin\theta)$, respectively.

In view of the above estimate for $\Lambda(m, \mathcal{I}(K))$, it seems we should make r as bigger as possible. Hence we should ask for the largest disk contained in $S(K)$. If $S(K)$ is star-shaped to certain point x_0, then r equals to the smallest distance from x_0 to the boundary of $S(K)$ because $S(K)$ is a polygon.

It remains to find an upper bound for $\#\mathcal{I}(K)$, which is a direct consequence of the assumptions on the triangulation $\mathcal{T}_h$ and the assumption on the element patch $S(K)$.

Lemma 6 *If* **Assumptions A1** *and* **A2** *on the triangulation* $\mathcal{T}_h$ *and* **Assumption A** *on the element patch* $S(K)$ *are valid, then we have*

$$\#\mathcal{I}(K) \le \sigma^2 \rho_1^2 R^2 / h_K^2. \tag{2.21}$$

Proof For any element $K \in \mathcal{T}_h$, using **Assumption A**, we obtain

$$\#S(K)\,|K| \le \pi R^2.$$

For any $\tau \in \widetilde{\mathcal{T}_h}|_K$, it is clear

$$|K| \ge |\tau| \ge \pi \rho_\tau^2.$$

Using **Assumption A1** and the consequence **M1**, we have

$$h_K \le \sigma \rho_1 \rho_\tau.$$

A combination of the above three inequalities gives (2.21) because $\#\mathcal{I}(K) = \#S(K)$. □

The upper bound (2.21) is independent of the approach for construction the element patch. For the two approaches based on the Moore neighbor and the von Neumann neighbor, we have $R \simeq t h_K$ with t the recursion depth. Hence we have $\#\mathcal{I}(K) \simeq t^2$, which is consistent with the upper bound proved in [32, Lemma 3.4], in which we have assumed that $S(K)$ is convex and the mesh is quasi-uniform. These two assumptions may be regarded as a special cases of the present assumption on $S(K)$ and the triangulation.

3 IPDG with Reconstructed Space for Poisson Problem

We shall use DG method with the reconstructed finite element space to solve second-order elliptic problem. For the sake of clarity and simplicity, we only consider the Poisson problem

$$-\triangle u = f \quad \text{in } \Omega, \qquad u = 0 \quad \text{on } \partial\Omega, \tag{3.1}$$

where Ω is a convex polygonal domain and f is a given function in $L^2(\Omega)$. The extension to the general second order elliptic problem is straightforward; see, e.g., the numerical examples in the next part. We also mention [33] for the implementation of this reconstructed finite element space together with the DG variational formulation in [37] to the biharmonic problem.

The approximating problem is to look for $u_h \in U_h$ such that

$$a_h(\mathcal{R}u_h, \mathcal{R}v) = (f, \mathcal{R}v)_h \quad \text{for all} \quad v \in U_h. \tag{3.2}$$

There are many different DG formulations for this problem as in [4] by specifying the bilinear form a_h and the source term $(f, \mathcal{R}v)_h$. To fix ideas, we focus on the IPDG method in [3],

where a_h and $(f, \mathcal{R}v)_h$ are defined for any $v, w \in V_h$ as

$$a_h(v, w) := \sum_{K\in\mathcal{T}_h} \int_K \nabla v \cdot \nabla w \, \mathrm{d}x - \sum_{e\in\mathcal{E}_h} \int_e (\llbracket \nabla v \rrbracket \{\{w\}\} + \llbracket \nabla w \rrbracket \{\{v\}\}) \, \mathrm{d}s + \sum_{e\in\mathcal{E}_h} \int_e \frac{\eta_e}{h_e} \llbracket v \rrbracket \cdot \llbracket w \rrbracket \mathrm{d}s,$$

and

$$(f, \mathcal{R}v)_h := \sum_{K\in\mathcal{T}_h} \int_K f(x)\mathcal{R}v(x) \, \mathrm{d}x,$$

where η_e is a piecewise positive constant. Here $\mathcal{E}_h$ is the collection of all edges of $\mathcal{T}_h$, and $\mathcal{E}_h^o$ is the collection of all the interior edges and $\mathcal{E}_h^\partial$ is the collection of all boundary edges. Moreover, the average $\{\{v\}\}$ and the jump $\llbracket v \rrbracket$ of v is defined as follows. Let e be a common edge shared by elements K_1 and K_2, and let n_1 and n_2 be the outward unit normal at e of K_1 and K_2, respectively. Given $v_i := v|_{\partial K_i}$, we define

$$\{\{v\}\} = \frac{1}{2}(v_1 + v_2), \quad \llbracket v \rrbracket = v_1 n_1 + v_2 n_2, \quad \text{on } e \in \mathcal{E}_h^o.$$

For a vector-valued function φ, we define φ_1 and φ_2 analogously and let

$$\{\{\varphi\}\} = \frac{1}{2}(\varphi_1 + \varphi_2), \quad \llbracket \varphi \rrbracket = \varphi_1 \cdot n_1 + \varphi_2 \cdot n_2, \quad \text{on } e \in \mathcal{E}_h^o.$$

For $e \in \mathcal{E}_h^\partial$, we set

$$\llbracket v \rrbracket = vn, \quad \{\{\varphi\}\} = \varphi.$$

We define the DG-energy norm for any $v \in V_h$ as

$$|\!|\!| v |\!|\!| = \left(\sum_{K\in\mathcal{T}_h} \| \nabla v \|^2_{L^2(K)} + \sum_{e\in\mathcal{E}_h} |e|^{-1} \| \llbracket v \rrbracket \|^2_{L^2(e)} \right)^{1/2}. \tag{3.3}$$

Using the *Agmon inequality* (2.1), the interpolation estimates (2.16) and (2.17), we obtain, for $g \in H^{m+1}(\Omega)$, there exists C that depends on N, σ, γ and m such that

$$|\!|\!| g - \mathcal{R}g |\!|\!| \le C(h^m + \Lambda_m d^m) \, | g |_{H^{m+1}(\Omega)}, \tag{3.4}$$

which implies that the nearly optimal approximation order of the reconstruction operator $\mathcal{R}$ is also valid for the DG-energy norm.

By definition, we obtain the consistency of a_h in the sense that

$$a_h(u, \mathcal{R}v) = (f, \mathcal{R}v)_h \quad \text{for all} \quad v \in U_h.$$

Therefore, the Galerkin orthogonality

$$a_h(u - \mathcal{R}u_h, \mathcal{R}v) = 0 \quad \text{for all} \quad v \in U_h \tag{3.5}$$

holds true. This is the starting point of the error estimate.

By *the discrete trace inequality* (2.5), for sufficiently large η_e, there exist Λ and λ that depend on N, σ, γ and m such that

$$\begin{aligned} a_h(\mathcal{R}v, \mathcal{R}v) &\geq \lambda |\!|\!| \mathcal{R}v |\!|\!|^2 && \text{for all} \quad v \in U_h, \\ |a_h(\mathcal{R}v, \mathcal{R}w)| &\leq \Lambda |\!|\!| \mathcal{R}v |\!|\!| |\!|\!| \mathcal{R}w |\!|\!| && \text{for all} \quad v, w \in U_h. \end{aligned}$$

This immediately gives the well-posedness of the approximating problem (3.2). The error estimate is given in the following theorem.

Theorem 1 *Let u and u_h be the solutions of* (3.1) *and* (3.2)*, respectively. If* **Assumption B** *holds, then*

$$|\!|\!| u - \mathcal{R}u_h |\!|\!| \leq (1 + \Lambda/\lambda) |\!|\!| u - \mathcal{R}u |\!|\!|. \tag{3.6}$$

And if $u \in H^{m+1}(\Omega)$, then there exists C that depends on N, σ, γ and m such that

$$|\!|\!| u - \mathcal{R}u_h |\!|\!| \leq C \left(h^m + \Lambda_m d^m\right) | u |_{H^{m+1}(\Omega)}, \tag{3.7}$$

and

$$\| u - \mathcal{R}u_h \|_{L^2(\Omega)} \leq C \left(h^m + \Lambda_m d^m\right) (h + d) | u |_{H^{m+1}(\Omega)}. \tag{3.8}$$

Remark 4 If **Assumption A** is valid, then we may reshape the above two estimates into

$$\| u - \mathcal{R}u_h \|_{L^2(\Omega)} + h |\!|\!| u - \mathcal{R}u_h |\!|\!| \leq C h^{m+1} | u |_{H^{m+1}(\Omega)}, \tag{3.9}$$

where C depends on N, σ, γ, m and the recursion depth t of the element patch.

If the element patch $S(K)$ is convex, then the above error estimate (3.9) remains true, while C depends on N, σ, m and t but is independent of the chunkiness parameter γ; cf., Remark 2.

Proof Denote $v = \mathcal{R}u - \mathcal{R}u_h$, we obtain

$$a_h(v, v) = a_h(\mathcal{R}u - u, v) + a_h(u - \mathcal{R}u_h, v) = a_h(\mathcal{R}u - u, v),$$

where we have used the Galerkin orthogonality (3.5) in the last step. This implies

$$|\!|\!| \mathcal{R}u - \mathcal{R}u_h |\!|\!| \leq \frac{\Lambda}{\lambda} |\!|\!| u - \mathcal{R}u |\!|\!|,$$

which together with the triangle inequality implies (3.6).

Substituting the approximation estimate (3.4) into (3.6), we obtain (3.7).

To show the L^2-error estimate (3.8), we use the standard duality argument. Let ϕ be the solution of

$$-\triangle \phi = u - \mathcal{R}u_h \quad \text{in } \Omega \qquad \phi = 0 \quad \text{on } \partial\Omega.$$

Using an integration by parts, the Galerkin orthogonality (3.5) and the interpolation estimate (3.4) with $m = 1$, we obtain

$$\begin{aligned} \| u - \mathcal{R}u_h \|^2_{L^2(\Omega)} &= \int_\Omega -\triangle\phi (u - \mathcal{R}u_h) \, \mathrm{d}x = a_h(u - \mathcal{R}u_h, \phi) \\ &= a_h(u - \mathcal{R}u_h, \phi - \mathcal{R}\phi) \\ &\leq \Lambda |\!|\!| u - \mathcal{R}u_h |\!|\!| |\!|\!| \phi - \mathcal{R}\phi |\!|\!| \\ &\leq C(h + d) |\!|\!| u - \mathcal{R}u_h |\!|\!| \, | \phi |_{H^2(\Omega)}. \end{aligned}$$

Next, as Ω is convex, elliptic regularity gives $| \phi |_{H^2(\Omega)} \leq C_r \| u - \mathcal{R}u_h \|_{L^2(\Omega)}$ with C_r depending only on the domain Ω. Hence, using the energy estimate (3.7), we obtain the L^2-error estimate (3.8). This completes the proof. □

4 Numerical Examples

In this section, we present a series of numerical examples showing the rates of convergence. We consider the general second order elliptic problem:

$$-\nabla\cdot(A(x)\nabla u(x)) = f(x) \tag{4.1}$$

supplemented with various boundary conditions. Here A is a two by two matrix that satisfies the ellipticity condition:

$$c_1(\xi_1^2+\xi_2^2) \le \sum_{i,j=1}^{2} A_{ij}(x)\xi_i\xi_j \le c_2\left(\xi_1^2+\xi_2^2\right) \quad \text{a.e. } x\in\Omega, \tag{4.2}$$

where $0 < c_1 \le c_2$ and $\xi_1, \xi_2 \in \mathbb{R}$. The bilinear form a_h in (3.2) is changed to

$$\begin{aligned} a_h(v,w) := &\sum_{K\in\mathcal{T}_h}\int_K A(x)\nabla v\cdot\nabla w\,\mathrm{d}x - \sum_{e\in\mathcal{E}_h}\int_e \left(\llbracket A\nabla v\rrbracket\{\{w\}\} + \llbracket A\nabla w\rrbracket\{\{v\}\}\right)\mathrm{d}s \\ &+ \sum_{e\in\mathcal{E}_h}\int_e \frac{\eta_e}{h_e}\llbracket v\rrbracket\cdot\llbracket w\rrbracket \mathrm{d}s \quad \text{for all } v, w\in V_h, \end{aligned}$$

and $(f, \mathcal{R}_h v)$ is unchanged for homogeneous boundary condition, and has to be modified for inhomogeneous boundary conditions accordingly.

In all the examples below, we take the penalty term η_e large enough to guarantee the coercivity of a_h. To be more precise, we let $\eta_e \ge 3c_2$ for the interior edges $e \in \mathcal{E}_h^o$, where c_2 is the ellipticity constant in (4.2); and η_e is taken as km^2 for boundary edge $e \in \mathcal{E}_h^\partial$ with m the reconstruction order and k a positive constant, while k may vary for different examples. A direct solver is employed to solve all the resulting linear systems.

The Assumptions **A1** and **A2** on the mesh can be visually checked by inspection on Figs. 4 and 7, while the validity of **Assumptions A** and **B** on the element patch does not seem easy to be checked for these meshes. We shall explain why both assumptions are true for the triangulations used in the first example, others may be proceeded similarly. For all the examples in this part, we construct the element patch by adding Von Neumann neighbors in a recursive way. The threshold c_0 is assigned a value which are mostly located in the interval $[1.5\dim\mathbb{P}_m, 2\dim\mathbb{P}_m]$, which will be specified later.

Example 1 In this example, we consider a 2D Laplace equation with homogeneous Neumann boundary condition posed on the unit square $\Omega = (0,1)^2$, i.e., $A(x)$ is a 2×2 identity matrix. An exact solution and a smooth source term f are assumed to be

$$u(x,y) = \sin(2\pi x)\sin(2\pi y) \quad \text{and} \quad f = 8\pi^2\sin(2\pi x)\sin(2\pi y).$$

In this case, a_h and $(f, \mathcal{R}_h v)$ have changed in the boundary which impose the boundary condition naturally. Meanwhile, the solution is determined up to a constant, to obtain a unique solution, we assume that the integral of the solution over the domain is zero. The first row and the first column of the resulting linear system are modified, and the numerical solution is corrected by the integral constraint.

We consider quasi-uniform triangular and quadrilateral meshes as shown in Fig. 4, which are generated by *Gmsh* [26]. The meshes are not sequentially refined from a common background mesh. Instead, the meshes are generated by a direct partition of the domain. We control the mesh size of the elements abutting the domain boundary to represent the mesh

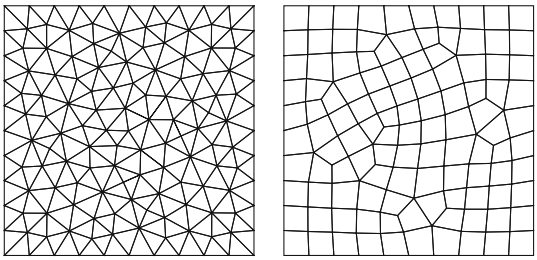

Fig. 4 The triangular and quadrilateral meshes for Example 1

Table 1 The number $\#S(K)$

Reconstruction order m	1	2	3	4	5	6
$\#S(K)$						
Example 1 (tri)	4	9	16	21	29	37
Example 1 (quad)	5	9	13	19	27	35
Example 2	7	13	22	29	35	43
Example 3	5	11	16	22	29	39

tri triangular, *quad* quadrilateral

size h of the triangulation. The mesh size h is halved each time from 0.1 to 0.00625 in order to simulate the effect of *uniform refinement*.

Firstly we list $\#S(K)$ in Table 1 for all the meshes we used in this part, which are mostly located in $[3(m+2)(m+1)/4, (m+2)(m+1)]$. We take the first order reconstruction as an example to explain how to check **Assumptions A** and **B** for the triangulations. The patch $S(K)$ is star-shaped with respect a point $x \in S(K)$ if every straight ray emanating from x intersects $\partial S(K)$ only once. In the first order approximation $S(K)$ includes at least all the Von Neumann neighbors of K, which allows us to take the inscribe circle of K as B_r. Figure 3 shows that larger $S(K)$ brings in larger B_r.

Assumption B is satisfied if the sampling nodes are not located in the zero set of a polynomial with the reconstruction order. For the first order reconstruction, this condition means that all the sampling nodes are not located in a straight line, this is possible due to the shape of $S(K)$. As to the high order reconstruction, it seems quite complicated to check such condition. Nevertheless, if we take the number $\#S(K)$ large enough, it does not seem possible that all the sampling nodes are all located in the zero set of a polynomial.

We report the numerical errors and the rates of convergence in Tables 2 and 3 for the triangular and quadrilateral meshes, respectively. It is clear that the method converges in the energy norm with rate m and converges in L^2 norm with rate $m+1$, where m is the reconstruction order, which is consistent with the theoretical prediction in Theorem 1. We also plot the rates of convergence in Figs. 5 and 6 for the triangular and quadrilateral meshes, respectively.

Example 2 This example is taken from [10, Example 4.1]. We consider the Dirichlet boundary value problem in the unit square $(0, 1)^2$ with the exact solution

$$u(x, y) = x^3 y^2 + x \sin(2\pi xy) \sin(2\pi y).$$

The coefficient matrix A is taken as

$$A(x, y) = \begin{pmatrix} (x+1)^2 + y^2 & -xy \\ -xy & (x+1)^2 \end{pmatrix}.$$

Table 2 Errors and rates of convergence on the triangular mesh for Example 1

m	Norms	h = 1.0e−1 error	5.0e−2 error	2.5e−2 error	1.25e−2 error	6.25e−3 error	Rate
1	$\| u - u_h \|_{L^2}$	2.10e−02	4.98e−03	1.24e−03	3.14e−04	7.73e−05	2.02
	$\|\| u - u_h \|\|$	1.23e+00	6.10e−01	3.06e−01	1.52e−01	7.58e−02	1.01
2	$\| u - u_h \|_{L^2}$	6.32e−03	7.40e−04	9.26e−05	1.20e−05	1.48e−06	3.00
	$\|\| u - u_h \|\|$	3.56e−01	8.91e−02	2.25e−02	5.87e−03	1.45e−03	1.98
3	$\| u - u_h \|_{L^2}$	1.80e−03	1.05e−04	6.18e−06	3.91e−07	2.34e−08	4.05
	$\|\| u - u_h \|\|$	1.01e−01	1.22e−02	1.47e−03	1.85e−04	2.25e−05	3.03
4	$\| u - u_h \|_{L^2}$	6.32e−04	1.54e−05	4.21e−07	1.34e−08	4.05e−10	5.13
	$\|\| u - u_h \|\|$	3.38e−02	1.81e−03	9.93e−05	6.27e−06	3.81e−07	4.10
5	$\| u - u_h \|_{L^2}$	2.21e−04	2.35e−06	2.86e−08	4.39e−10	6.36e−12	6.25
	$\|\| u - u_h \|\|$	1.28e−02	3.15e−04	7.33e−06	2.25e−07	6.38e−09	5.23
6	$\| u - u_h \|_{L^2}$	6.73e−05	5.16e−07	2.54e−09	1.80e−11	1.38e−13	7.25
	$\|\| u - u_h \|\|$	4.20e−03	8.45e−05	7.22e−07	9.23e−09	1.39e−10	6.28

Table 3 Errors and rates of convergence on the quadrilateral mesh for Example 1

m	Norms	h = 1.0e−1 error	5.0e−2 error	2.5e−2 error	1.25e−2 error	6.25e−3 error	Rate
1	$\| u - u_h \|_{L^2}$	3.30e−02	7.41e−03	1.78e−03	4.47e−04	1.06e−04	2.01
	$\|\| u - u_h \|\|$	1.51e+00	6.93e−01	3.48e−01	1.73e−01	8.44e−02	1.01
2	$\| u - u_h \|_{L^2}$	1.88e−02	2.01e−03	2.37e−04	3.05e−05	3.77e−06	3.06
	$\|\| u - u_h \|\|$	7.70e−01	1.73e−01	4.35e−02	1.13e−02	2.83e−03	2.01
3	$\| u - u_h \|_{L^2}$	1.43e−02	4.48e−04	2.25e−05	1.27e−06	7.47e−08	4.35
	$\|\| u - u_h \|\|$	4.35e−01	3.48e−02	3.82e−03	4.51e−04	5.30e−05	3.22
4	$\| u - u_h \|_{L^2}$	1.25e−02	1.16e−04	2.40e−06	7.68e−08	2.23e−09	5.53
	$\|\| u - u_h \|\|$	2.95e−01	9.01e−03	4.00e−04	2.47e−05	1.46e−06	4.37
5	$\| u - u_h \|_{L^2}$	6.31e−03	2.56e−05	3.66e−07	5.32e−09	6.53e−11	6.52
	$\|\| u - u_h \|\|$	1.93e−01	2.16e−03	6.16e−05	1.66e−06	4.15e−08	5.46
6	$\| u - u_h \|_{L^2}$	2.37e−03	6.44e−06	4.32e−08	3.56e−10	2.65e−12	7.36
	$\|\| u - u_h \|\|$	8.43e−02	5.07e−04	7.10e−06	1.06e−07	1.45e−09	6.38

The force f is then determined by (4.1). We solve this problem over a sequence of hexagonal meshes as shown in Fig. 7, which are generated by a Voronoi tessellation. The details for mesh construction may also be found in [10, Example 4.1]. The mesh contains elements with different shapes such as hexagons, pentagons, and quadrilaterals. It seems different element shape does not bring in extra difficulties in implementation. We use the total number of the elements given in Fig. 7 to be 115, 430, 1660, 6520 and 25800 ro simulate the effect of *uniform refinement*. Numerical error and the rates of convergence are reported in Table 4 and Fig. 8, respectively, which are also agreed with the theoretical prediction.

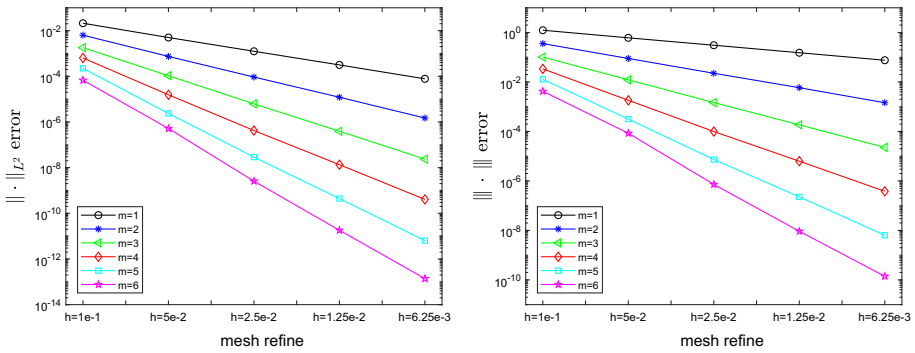

Fig. 5 The rates of convergence in L^2 norm (left) and the energy norm (right) for different reconstruction order m on triangular mesh for Example 1

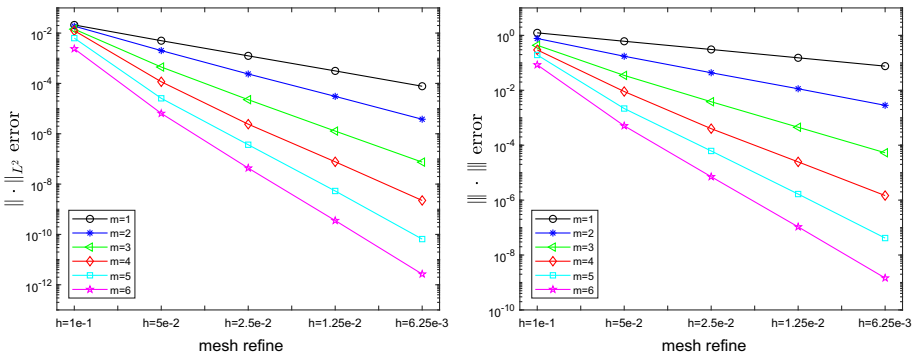

Fig. 6 Rates of convergence in L^2 norm (left) and the energy norm (right) for different reconstruction order m on quadrilateral mesh for Example 1

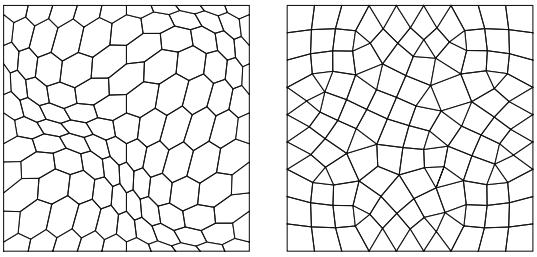

Fig. 7 The hexagonal mesh and the mixed mesh for Examples 2 and 3

Example 3 We consider a Neumann boundary value problem in the unit square with the exact solution

$$u(x, y) = \exp\left(\frac{x^2 + y^2}{2}\right) + \sin[2\pi(x + y)]\sin(2\pi y),$$

and we take the coefficients matrix as

$$A(x, y) = \begin{pmatrix} 3 + \cos(2\pi x) & x - y \\ x - y & 3 - \sin(2\pi y) \end{pmatrix}.$$

Table 4 Errors and rates of convergence on the hexagonal mesh for Examples 2

m	Norms	N = 1.15e+2 error	4.30e+2 error	1.66e+3 error	6.52e+3 error	2.58e+4 error	Rate
1	$\|u-u_h\|_{L^2}$	3.91e−02	1.11e−02	2.87e−03	7.17e−04	1.79e−04	1.95
	$\|\|\|u-u_h\|\|\|$	1.53e+00	7.67e−01	3.82e−01	1.97e−01	1.01e−01	0.98
2	$\|u-u_h\|_{L^2}$	3.35e−02	4.50e−03	5.42e−04	6.94e−05	8.57e−06	2.99
	$\|\|\|u-u_h\|\|\|$	1.41e+00	4.36e−01	1.11e−01	2.87e−02	7.15e−03	1.92
3	$\|u-u_h\|_{L^2}$	1.58e−02	1.29e−03	7.48e−05	4.41e−06	2.69e−07	3.99
	$\|\|\|u-u_h\|\|\|$	7.67e−01	1.07e−01	1.35e−02	1.64e−03	1.94e−04	2.99
4	$\|u-u_h\|_{L^2}$	1.42e−02	5.09e−04	1.48e−05	4.61e−07	1.47e−08	4.99
	$\|\|\|u-u_h\|\|\|$	5.53e−01	4.73e−02	2.83e−03	1.79e−04	1.17e−05	3.91
5	$\|u-u_h\|_{L^2}$	1.28e−02	3.65e−04	6.89e−06	1.02e−07	1.54e−09	5.77
	$\|\|\|u-u_h\|\|\|$	4.68e−01	3.40e−02	1.23e−03	3.71e−05	1.04e−06	4.74
6	$\|u-u_h\|_{L^2}$	9.45e−03	1.59e−04	1.28e−06	1.04e−08	7.33e−11	6.78
	$\|\|\|u-u_h\|\|\|$	3.17e−01	1.31e−02	2.23e−04	3.65e−06	5.58e−08	5.67

N is the number of the total degrees of freedom

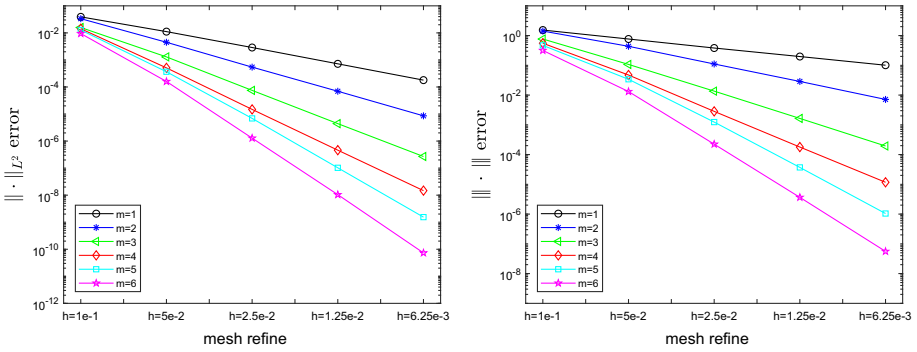

Fig. 8 The rates of convergence in L^2 norm (left) and the energy norm (right) for different reconstruction order m over hexagonal mesh for Example 2

In this example, we have to modify $(f, \mathcal{R}_h v)$ by including the inhomogeneous boundary flux as

$$(f, \mathcal{R}_h v) = \sum_{K \in \mathcal{T}_h} f \mathcal{R}_h v \, \mathrm{d}x + \sum_{e \in \mathcal{E}_h^b} \int_e \frac{\partial u}{\partial n} v \mathrm{d}s.$$

The mesh is generated by *Gmsh* [26] again, which contains both triangles and quadrilaterals as shown in Fig. 7. In this example, the sampling points are randomly selected inside the element instead of the element barycenters. We perturb each barycenter with a uniform distribution random vector $\xi \in \mathbb{R}^2$ with $|\xi| = 0.1 h_K$, which guarantees the perturbed sampling points are still located in the interior of the corresponding element. We show in Fig. 3 an example of the perturbed sampling points.

Errors and rates of convergence are given in Table 5 and Fig. 9. Again we achieved the same rates of convergence as that in the previous examples. This indicates that the method is robust with respect to the perturbation of the sampling points as shown in Lemma 3.

Table 5 Errors and the rates of convergence for Example 3

m	Norms	N = 1.29e+2 error	5.10e+2 error	2.33e+3 error	9.24e+3 error	3.80e+4 error	Rate
1	$\|u-u_h\|_{L^2}$	6.66e−02	1.48e−02	3.47e−03	8.27e−04	2.01e−04	2.07
	$\|\|\|u-u_h\|\|\|$	3.35e+00	1.57e+00	8.44e−01	4.04e−01	2.02e−01	0.99
2	$\|u-u_h\|_{L^2}$	4.76e−02	6.68e−03	7.00e−04	9.29e−05	1.08e−05	3.04
	$\|\|\|u-u_h\|\|\|$	2.17e+00	7.12e−01	1.59e−01	4.28e−02	1.00e−02	1.96
3	$\|u-u_h\|_{L^2}$	3.11e−02	1.81e−03	8.04e−05	4.85e−06	2.69e−07	4.22
	$\|\|\|u-u_h\|\|\|$	1.24e+00	1.82e−01	1.82e−02	2.25e−03	2.56e−04	3.08
4	$\|u-u_h\|_{L^2}$	1.63e−02	7.26e−04	1.42e−05	4.63e−07	1.26e−08	5.12
	$\|\|\|u-u_h\|\|\|$	7.55e−01	7.29e−02	3.12e−03	2.06e−04	1.13e−05	4.05
5	$\|u-u_h\|_{L^2}$	1.27e−02	3.31e−04	2.95e−06	3.84e−08	5.62e−10	6.19
	$\|\|\|u-u_h\|\|\|$	5.73e−01	3.54e−02	7.10e−04	1.88e−05	5.23e−07	5.10
6	$\|u-u_h\|_{L^2}$	1.76e−02	2.09e−04	1.21e−06	8.66e−09	2.99e−11	7.28
	$\|\|\|u-u_h\|\|\|$	1.10e+00	2.07e−02	3.36e−04	4.74e−06	2.97e−08	6.24

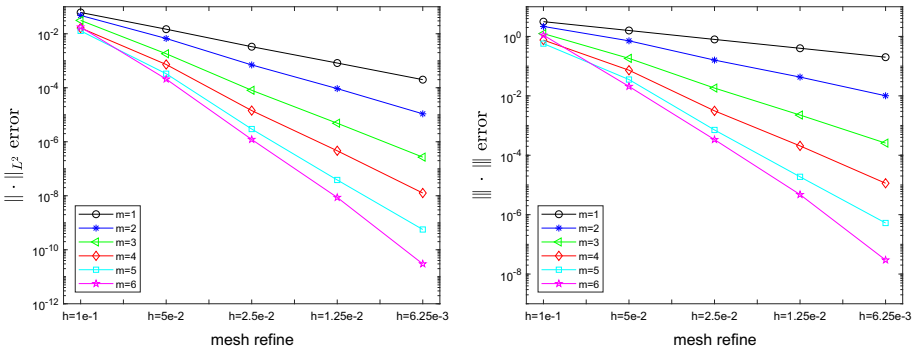

Fig. 9 The rates of convergence in L^2 norm (left) and the energy norm (right) for different m for Example 3

5 Conclusions

Using a least-squares patch reconstruction, we construct a new discontinuous finite element space over polygonal mesh, which together with the variational formulation of DG method gives a new approximation method for partial differential equations. A novelty of this method is that arbitrary-order accuracy has been achieved with only one degree of freedom on each element, while the shape of the element may be arbitrary. Optimal error estimates have been proved and a variety of numerical examples demonstrate the superior performance of the method. It would be interesting to consider the $h-m$ version of the proposed method and the corresponding adaptive refinement strategy, and to consider the efficient solver for the resulting linear algebra system, and to consider the choice of the interior penalty parameter that allow for edge/face degeneration as in [12], which is key for implementation the method on more general polytopic mesh. Moreover, the assumption on the element patch may be further weakened, which may render more flexibility for the method. We shall leave all these issues to further exploration.

Acknowledgements The authors would like to thank Dr. Fengyang Tang for his help in the earlier stage of the present work, and the authors would like to thank the anonymous referees for the constructive comments that improve the paper. Funding was provided by National Natural Science Foundation of China (Grant Nos. 11425106, 91630313, 91630313, 11671312)

References

1. Adams, R.A., Fournier, J.J.F.: Sobolev Spaces, 2nd edn. Elsevier, Amsterdam (2003)
2. Antonietti, P.F., Giani, S., Houston, P.: *hp*-version composite discontinuous Galerkin methods for elliptic problems on complicated domains. SIAM J. Sci. Comput. **35**, A1417–A1439 (2013)
3. Arnold, D.N.: An interior penalty finite element method with discontinuous elements. SIAM J. Numer. Anal. **19**, 742–760 (1982)
4. Arnold, D.N., Brezzi, F., Cockburn, B., Marini, L.D.: Unified analysis of discontinuous Galerkin methods for elliptic problems. SIAM J. Numer. Anal. **39**, 1749–1779 (2002)
5. Banks, J., Hagstrom, T.: On Galerkin difference methods. J. Comput. Phys. **313**, 310–327 (2016)
6. Barth, T.J., Larson, M.G.: A posteriori error estimates for higher order Godunov finite volume methods on unstructured meshes. Finite volumes for complex applications, III (Porquerolles, 2002), pp. 27–49. Hermes Sci. Publ, Paris (2002)
7. Bassi, F., Botti, L., Colombo, A., Rebay, S.: Agglomeration-based discontinuous galerkin discretization of Euler and Navier–Stokes equations. Comput. Fluids **61**, 77–85 (2012)
8. Bassi, F., Botti, L., Colombo, A.: Agglomeration-based physical frame dG discretization: an attempt to be mesh free. Math. Models Methods Appl. Sci. **24**, 1495–1539 (2014)
9. Brenner, S.C., Scott, L.R.: The Mathematical Theory of Finite Element Methods, vol. 15, 3rd edn. Springer, New York (2008)
10. Brezzi, F., Lipnikov, K., Simoncini, V.: A family of mimetic finite difference methods on polygonal and polyhedral meshes. Math. Models Methods Appl. Sci. **15**, 1533–1551 (2005)
11. Brezzi, F., Buffa, A., Lipnikov, K.: Mimetic finite differences for elliptic problems. ESAIM Numer. Anal. **43**, 277–295 (2009)
12. Cangiani, A., Georgoulis, E.H., Houston, P.: *hp*-version discontinuous Galerkin methods on polygonal and polyhedral meshes. Math. Models Methods Appl. Sci. **24**, 2009–2041 (2014)
13. Cangiani, A., Dong, Z.N., Georgoulis, E.H., Houston, P.: hp-version discontinuous galerkin methods for advection–diffusion–reaction problems on polytopic meshes. ESAIM Math. Model. Numer. Anal. **50**, 699–725 (2016)
14. Cangiani, A., Dong, Z.N., Georgoulis, E.H., Houston, P.: hp-Version Discontinuous Galerkin Methods on Polygonal and Polyhedral Meshes. SpringerBriefs in Mathematics. Springer, Berlin (2017)
15. Chen, H.T., Guo, H.L., Zhang, Z.M., Zou, Q.S.: A C^0 linear finite element method for two fourth order eigenvalue problems. IAM J. Numer. Anal. **37**, 2120–2138 (2017)
16. Ciarlet, P.G.: The Finite Element Method for Elliptic Problems. North-Holland, Amsterdam (1978)
17. Clément, P.: Approximation by finite element functions using local regularization. RAIRO Anal. Numér. **9**, 77–84 (1975)
18. Cockburn, B., Karniadakis, G.E., Shu, C.W.: The development of discontinuous Galerkin methods. In: Newport, R.I. (ed.) Discontinuous Galerkin Methods, Lect. Notes Comput. Sci. Eng., vol. 11, pp. 3–50. Springer, Berlin (1999)
19. Cockburn, B., Gopalakrishnan, J., Lazarov, R.: Unified hybridization of discontinuous Galerkin, mixed, and continuous Galerkin methods for second order elliptic problems. SIAM J. Numer. Anal. **47**, 1319–1365 (2009)
20. da Veiga, L.B., Lipnikov, K., Manzini, G.: The Mimetic Finite Difference Method for Elliptic Problems, MS&A. Modeling, Simulation and Applications, vol. 11. Springer, Cham (2014)
21. Dekel, S., Leviatan, D.: The Bramble–Hilbert lemma for convex domains. SIAM J. Math. Anal. **35**, 1203–1212 (2004)
22. Di Pierto, D.A., Ern, A.: Mathematical Aspects of Discontinuous Galerkin Methods, vol. 69. Springer, Berlin (2012)
23. Di Pierto, D.A., Ern, A., Lemaire, S.: An arbitrary-order and compact-stencil discretization of diffusion on general meshes based on local reconstruction operators. Comput. Methods Appl. Math. **14**, 461–472 (2014)
24. Dupont, T., Scott, L.R.: Polynomial approximation of functions in Sobolev spaces. Math. Comput. **34**, 441–463 (1980)

25. Georgoulis, E., Pryer, T.: Recovered finite element methods. Comput. Methods Appl. Mech. Eng. **332**, 303–324 (2018)
26. Geuzaine, C., Remacle, J.F.: Gmsh: a 3-D finite element mesh generator with built-in pre- and post-processing facilities. Int. J. Numer. Methods Eng. **79**, 1309–1331 (2009)
27. Grisvard, P.: Elliptic Problems in Nonsmooth Domains. Pitman, Boston (1985)
28. Guo, H.L., Zhang, Z.M., Zou, Q.S.: A C^0 linear finite element method for biharmonic problems. J. Sci. Comput. **74**, 1397–1422 (2018)
29. Hampshire, J.K., TBH, V., CH, C.: Three node triangular bending elements with one degree of freedom per node. Eng. Comput. **9**(1), 49–62 (1992)
30. Hesthaven, J.S., Warburton, T.: Nodal Discontinuous Galerkin Methods: Algorithms, Analysis, and Applications, p. 233. Springer, Berlin (2008)
31. Larsson, K., Larson, M.G.: Continuous piecewise linear finite elements for the Kirchhoff–Love plate equation. Numer. Math. **121**, 65–97 (2012)
32. Li, R., Ming, P.B., Tang, F.Y.: An efficient high order heterogeneous multiscale method for elliptic problems. Multiscale Model. Simul. **10**, 259–283 (2012)
33. Li, R., Ming, P.B., Sun, Z.Y., Yang, F.Y., Yang, Z.J.: A discontinuous Galerkin method by patch reconstruction for biharmonic problem. J. Comput. Math. **37**, 561–578 (2019a)
34. Li, R., Sun, Z.Y., Yang, F.Y.: Solving eigenvalue problems in a discontinuous Galerkin approximate space by patch reconstruction (2019b). arXiv:1901.01803
35. Li, R., Sun, Z.Y., Yang, F.Y., Yang, Z.J.: A finite element method by patch reconstruction for the Stokes problem using mixed formulations. J. Comput. Appl. Math. **353**, 1–20 (2019c)
36. Lipnikov, K., Vassilev, D., Yotov, I.: Discontinuous Galerkin and mimetic finite difference methods for coupled Stokes–Darcy flows on polygonal and polyhedral grids. Numer. Math. **126**, 1–40 (2013)
37. Mozolevski, I., Süli, E.: A priori error analysis for the *hp*-version of the discontinuous Galerkin finite element method for the biharmonic equation. Comput. Methods Appl. Math. **3**, 596–607 (2003)
38. Mu, L., Wang, J.P., Wang, Y.Q., Ye, X.: Interior penalty discontinuous Galerkin method on very general polygonal and polyhedral meshes. J. Comput. Appl. Math. **255**, 432–440 (2014)
39. Narcowich, F.J., Ward, J.D., Wendland, H.: Sobolev bounds on functions with scattered zeros, with applications to radial basis function surface fitting. Math. Comput. **74**, 743–763 (2005)
40. Nay, R.A., Utku, S.: An alternative for the finite element method. In: Variational Methods in Engineering, vol. 1. University of Southampton (1972)
41. Oñate, E., Cervera, M.: Derivation of thin plate bending elements with one degree of freedom per node: a simple three node triangle. Eng. Comput. **10**, 543–561 (1993)
42. Phaal, R., Calladine, C.R.: A simple class of finite elements for plate and shell problems. II: an element for thin shells, with only translational degrees of freedom. Int. J. Numer. Methods Eng. **35**, 979–996 (1992)
43. Reed, W.H., Hill, T.R.: Triangular Mesh Methods for the Neutron Transport Equation. Tech. Report LA-UR-73-479, Los Alamos Scientific Laboratory (1973)
44. Reichel, L.: On polynomial approximation in the uniform norm by the discrete least squares method. BIT **26**, 349–368 (1986)
45. Sukumar, N., Tabarraei, A.: Conforming polygonal finite elements. Int. J. Numer. Methods Eng. **61**, 2045–2066 (2004)
46. Sullivan, D.O.: Exploring spatial process dynamics using irregular cellular automaton models. Geogr. Anal. **33**, 1–18 (2001)
47. Venkatakrishnan, V.: Convergence to steady state solutions of the Euler equations on unstructured grids with limiters. J. Comput. Phys. **118**, 120–130 (1995)
48. Wendland, H.: Scattered Data Approximation. Cambridge Univeristy Press, Cambridge (2005)
49. Wilhelmsen, D.: A Markov inequality in several dimensions. J. Approx. Theory **11**, 216–220 (1974)
50. Wirasaet, D., Kubatko, E.J., Michoski, C.E., Tanaka, S., Westerink, J.J., Dawson, C.: Discontinuous Galerkin methods with nodal and hybrid modal/nodal triangular, quadrilateral, and polygonal elements for nonlinear shallow water flow. Comput. Methods Appl. Mech. Eng. **270**, 113–149 (2014)
51. Yamakawa, S., Shimada, K.: Converting a tetrahedral mesh to a prism-tetrahedral hybrid mesh for FEM accuracy and efficiency. Int. J. Numer. Methods Eng. **80**, 2099–2129 (2009)